scientific reports

Check for updates

OPEN

Modeling the metastatic tumor microenvironment: a co-culture platform of lung cancer and blood vessel organoids for drug evaluation

Mingyun Lee[1], Yeo-Joon Yoon[1], Ji Yeon Lee[1], Mina Hwang[3], Sewon Park[6], Min Hak Lee[7], Sang-Won Um[3,4], Byoung Chul Cho[5,6], Jinguen Rheey[1], Toshiro Sato[2] & Yong Soo Lee[1]✉

Tumor cell–vasculature interactions play a crucial role in lung cancer progression and metastasis; however, traditional cell culture models rarely capture these complex dynamics. We developed a vascularized lung cancer organoid (VLCO) model by coculturing lung cancer organoids (LCOs) with blood vessel organoids (BVOs) to recreate the tumor–vasculature niche in a three-dimensional in vitro system. During coculture, LCOs migrated along BVO-formed vascular networks and invaded vessel-like structures, mimicking intravasation. The organoid types interacted via secretory factors, including TGF-β and PDGF-BB, inducing epithelial–mesenchymal transition (EMT) in LCOs and pericyte-to-fibroblast transition in BVOs. We also developed a scalable drug response assay for vasculature-induced EMT, enabling targeted therapeutic screening. The VLCO model provides a robust platform for studying tumor–endothelial crosstalk and testing antimetastatic therapies targeting tumor–vasculature interactions.

Metastasis is a hallmark of cancer and a leading cause of mortality and therapy resistance[1]. It is a dynamic, multistep process in which cancer cells spread from primary tumors to distant organs, driven by biochemical and biophysical signals from the tumor microenvironment (TME)[2]. The TME regulates cancer cell behavior and contributes to matrix formation, supporting metastatic spread[3]. Blood vessels within the TME are critical for tumor progression, supplying nutrients and oxygen to promote proliferation, survival, and metastasis[4]. They also aid in matrix remodeling by providing matrix cells through endothelial–mesenchymal metastasis (EndMT) and pericyte-to-fibroblast transition (PFT)[5,6]. Despite their crucial role in metastasis, cancer cell–vasculature interactions remain poorly understood.

Numerous studies have examined the relationships between vascular components and cancer, particularly those involving endothelial and mesodermal progenitor cells. Coculture systems have been developed to model these interactions, including a four-dimensional organoid system that visualizes cancer cell invasion into blood vessels, offering insights into tumor–vasculature dynamics[7]. Additionally, in vitro models incorporating perfused vessels have highlighted the role of vascular perfusion in cancer progression[8]. More physiologically relevant platforms now integrate mesodermal progenitor cells, enabling the generation of complex human organoid models with vascular networks[9]. Although these studies emphasize the importance of vascular organ systems for studying vasculature–cancer interactions, early models often lacked the complexity to fully replicate vascular function or TME interactions. To address these limitations, Wimmer et al.[10] developed a three-dimensional (3D) model that more accurately mimics blood vessel structure and function.

[1]Gradiant Bioconvergence Inc., Songpa-Gu, Seoul, Republic of Korea. [2]Department of Integrated Medicine and Biochemistry, Keio University School of Medicine, Tokyo 160-8582, Japan. [3]Division of Pulmonary and Critical Care Medicine, Department of Medicine, Samsung Medical Center, Sungkyunkwan University School of Medicine, Seoul, Republic of Korea. [4]Department of Health Sciences and Technology, SAIHST, Sungkyunkwan University, Seoul, Republic of Korea. [5]Division of Medical Oncology, Yonsei Cancer Center, Yonsei University College of Medicine, Seoul, Republic of Korea. [6]Yonsei New Il Han Institute for Integrative Lung Cancer Research, Yonsei University College of Medicine, Seoul, Republic of Korea. [7]JEUK Institute for Cancer Research, JEUK Co., Ltd., Gumi-City, Kyungbuk, Republic of Korea. ✉email: yslee7@gradiantbio.com

Blood vessel organoids (BVOs) comprise diverse vascular cells, including endothelial cells, pericytes, and mesenchymal stem cells, each contributing to vascular integrity and structural remodeling. Advances in BVO coculture techniques have markedly improved the ability to model complex physiological and pathological processes. For example, coculturing BVOs with cerebral organoids generates functional neurovascular networks, providing insights into neurological diseases and blood–brain barrier dynamics[11,12]. Integrating BVOs with THP1 immune cells has facilitated effective modeling of inflammatory conditions, such as atherosclerosis[13]. In cancer research, BVOs replicate key blood vessel features, offering a robust platform for studying tumor–vasculature interactions that regulate the TME and metastatic progression. In parallel with this blood vessel development, organoid-based models have revolutionized cancer research by providing 3D structures that closely replicate tissue architecture[14].]. These models are particularly valuable for cancer research, as they enable the investigation of complex interactions among various cell types. Cancer organoids derived from patient tumors retain genetic and phenotypic properties, including heterogeneity, making them ideal for drug screening and translational studies[15]. Combining BVOs with cancer organoids can improve tumor–stroma interaction modeling, as demonstrated through coculturing BVOs with glioblastoma organoids, which revealed the antitumor potential of engineered immune cells in the TME[16]. By combining the patient-derived characteristics of cancer organoids with the structural and functional fidelity of BVOs, this coculture platform can closely mimic in vivo tumor–stroma interactions, potentially advancing cancer research and therapeutic development.

In this study, we identified fibroblast differentiation within the TME and examined signaling factors that induce epithelial–mesenchymal transition (EMT), stromal remodeling, and tumor fibrosis using gene expression and imaging techniques. We also evaluated EMT-inhibiting drugs in vasculature–lung cancer organoids to assess their potential as a drug testing platform. This model not only provides a powerful tool for studying metastasis in vitro but also lays the foundation for identifying novel therapeutic strategies to inhibit cancer metastasis.

Results

Intravasation modeling with lung cancer organoids and BVOs

To investigate interactions between lung cancer organoids (LCOs) and blood vessels in vitro, we first generated BVOs from induced pluripotent stem cells following the protocol established by Wimmer et al.[17]. These BVOs exhibited the expected structure and cellular composition (Figure S1). Subsequently, we cocultured LCOs and BVOs to create a combined organoid model. BVOs were dissociated into single cells, whereas LCOs were mechanically fragmented into small clumps, both of which were embedded together in a Matrigel dome (Fig. 1A). Immunostaining confirmed EpCAM and CD31 expression on the LCOs and BVO-derived vasculature, respectively, indicating successful incorporation of the tumor and vessel components in the coculture. Over 10 days of coculture, LCOs formed spherical clusters, whereas BVO cells developed extensive vascular networks (Fig. 1B). By day 15, the growing BVO network had extended and established contact with adjacent LCO structures, enabling LCOs to spread along the BVO-derived vascular networks on day 21.

Next, we sought to model cancer cell intravasation. To distinguish cancer cells from BVO-derived cells, we generated RFP-labeled LCOs from two tumor sources: one derived from a surgically resected primary tumor (sLCO) and one from a pleural effusion (pLCO). The intravasation capacity of the pLCO was presumed to be higher than that of the sLCO. Additionally, we modified the coculture conditions for the intravasation assay. Specifically, dissociated RFP-labeled LCO cells were cocultured with intact, undissociated BVOs, suspended in liquid Matrigel, and seeded in ultra-low-attachment U-bottom plates (Fig. 1C), allowing the cancer cells to move freely and interact with the preformed vascular structures (Fig. 1D). Under these conditions, migration rates of pLCO cells into the BVOs were significantly higher than those of sLCO cells. We further quantified invasion into BVOs by isolating composite organoids and dissociating them into single cells for analysis. Flow cytometry and image based analysis revealed that RFP-positive LCO cells outnumbered RFP-negative BVO cells, indicating substantial cancer cell entry into the BVOs (Fig. 1E, F). Collectively, these results demonstrate that the LCO–BVO coculture model successfully recapitulates cancer cell intravasation in vitro.

LCO and BVO undergo EMT and PFT during coculture

Regarding the mechanisms driving LCO migration and intravasation into BVOs, we hypothesized that the organoid types communicate via soluble factors. We tested this using a Transwell coculture system, which allows the exchange of secreted molecules while preventing direct cell contact. Relative to LCO monocultures, cocultured LCOs upregulated EMT-related genes[18,19], suggesting that coculture induces EMT in LCOs. Cocultured BVOs exhibited fibroblast marker (FSP1 and FAP) upregulation and pericyte marker (PDGFRβ and NG2) downregulation, indicative of PFT. These results suggest that LCOs and BVOs influence each other via soluble factors, inducing distinct gene expression changes. Consistent with prior reports, co-culture elevated TGF-β transcripts in BVOs and PDGF-BB transcripts in LCOs; functionally, these ligands act paracrinely to promote EMT in LCOs and PFT in BVOs, respectively. Consistent with previous reports linking TGF-β to EMT and PDGF-BB to PFT, gene expression analysis revealed increased TGF-β and PDGF-BB levels in cocultured BVOs and LCOs, respectively (Fig. 2A and Figure S2)[5,20,21]. ELISA confirmed higher concentrations of TGF-β and PDGF-BB in coculture supernatants compared with LCO or BVO monocultures. (Fig. 2B).

To determine whether direct coculture in a 3D matrix triggers PFT in BVO-derived cells, we performed immunofluorescence analysis of fibroblast markers in a Matrigel coculture. On day 15, LCO monocultures showed weak FSP1 staining, whereas BVO monocultures lacked FSP1 and FAP staining (Fig. 2C, D). In cocultures, PDGFRβ-positive BVO-derived cells were connected to LCOs but did not express FSP1 or FAP. On day 18, monocultures remained unchanged, but cocultures exhibited FSP1 and FAP expression in BVO-derived cells, with some coexpressing PDGFRβ (white arrows). Thus, over time, pericytes from BVOs transition into cancer-associated fibroblast (CAF)-like cells under LCO influence. Considering the present and previous

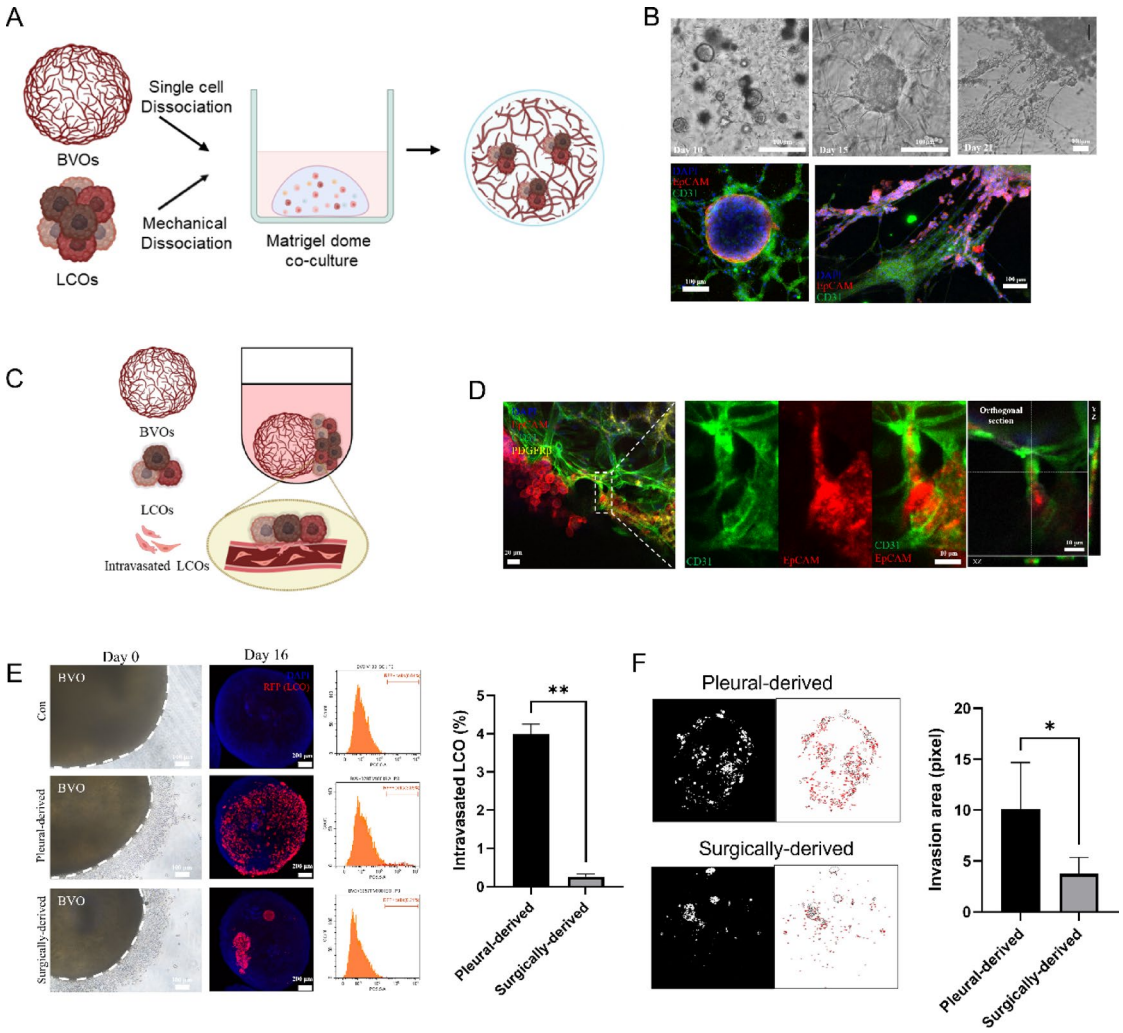

Fig. 1. Co-culture of BVOs and LCOs induces migration of LCOs. (**A**) Schematic representation of BVO and LCO co-culture in a Matrigel dome. Illustrations were created with BioRender. (**B**) Co-culture with BVOs induces LCO migration along vascular structures. Brightfield and immunocytochemistry images showing the progression of BVO (CD31, green) and LCO (EpCAM, red) co-culture at different time points (Day 10, Day 15, and Day 21). (**C**) Schematic representation of the intravasation assay using coculture. Illustrations were created with BioRender. (**D**) Immunofluorescence analysis of LCO marker (EpCAM, red), endothelial cell marker (CD31, green), and pericyte marker (PDGFRβ, yellow) on day 7 of intravasation assay and orthogonal projections (xy, xz, and yz). (**E**) Bright-field images of intravasation assay on day 0. Immunofluorescence imaging of intravasation assay on day 16 of coculture, showing RFP + LCOs and DAPI staining. Flow cytometry quantification of intravasated RFP + LCOs on Day 16. (**F**) Quantification of intravasated RFP + LCOs by image-based analysis on day 16 of co-culture. Statistical significance was evaluated by two-tailed unpaired t-test with $^{*}p < 0.05$, $^{**}p < 0.01$.

findings, we postulate that elevated TGF-β and PDGF-BB levels the coculture milieu drive mesenchymal conversion in cancer cells and vasculature, likely enhancing intravasation (Fig. 2E)[22–25].

VLCO model for assessing vasculature-induced EMT

Next, we developed a standardized platform to model vasculature-induced EMT as a proxy for intravasation. To streamline the assay, we dissociated BVOs and LCOs into single cells, plating them in ultra-low-attachment plates at an optimized ratio (Fig. 3A). Within 4 days, the cells self-assembled into composite organoids, i.e., assembloids. By day 5, RFP-labeled LCOs had begun migrating along the developing vasculature, progressively distributing throughout the BVO-derived vascular network (Fig. 3B and Figure S3). We termed this vascularized LCO–BVO assembloid the "VLCO" model.

To determine if LCOs in VLCOs undergo EMT, we analyzed EMT marker expression. RFP-labeled LCOs in VLCOs expressed ZEB2 and TWIST1, both EMT-related transcription factors, without exhibiting E-cadherin expression, indicative of EMT (Fig. 3C–E). In contrast, monocultured LCO cells retained E-cadherin expression but lacked EMT marker expression. A higher proportion of E-cadherin–negative cells in VLCOs relative to LCO moncultures was confirmed via flow cytometry (Fig. 3F). Notably, the mesenchymal marker N-cadherin was

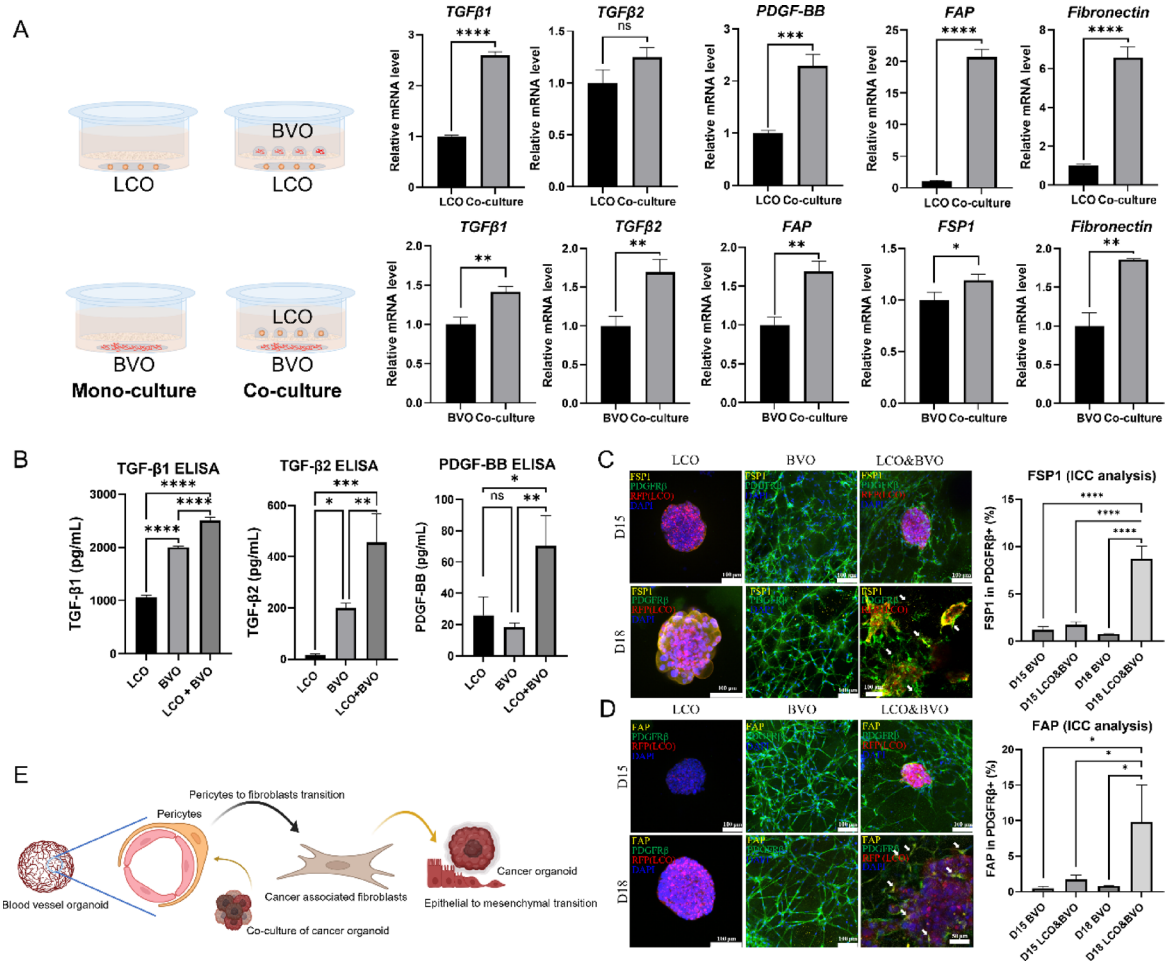

Fig. 2. Analysis of EMT induction and PFT in LCO-BVO co-culture systems. (**A**) Schematic representation and qPCR analysis of LCOs and BVOs cultured in a Transwell system with a 3 μm pore size for 12 days, comparing EMT-related gene expression in LCOs with PFT-related gene expression in BVOs under both monoculture and co-culture conditions. (**B**) ELISA assay measuring the levels of TGF-β1, TGF-β2, and PDGF-BB in culture supernatants from three different conditions: LCO monoculture, BVO monoculture, and LCO-BVO co-culture. (**C**) Immunocytochemistry analysis on day 15 and day 18 of Matrigel dome co-culture, showing fibroblast markers (FSP1, yellow) and the pericyte marker (PDGFRβ, green) in the presence of RFP + LCOs and DAPI staining. White arrows indicate FSP1 expression in BVOs. Quantification of fluorescence intensity shows the co-localization of FSP1 and PDGFRβ. (**D**) Immunocytochemistry analysis on day 15 and day 18 of Matrigel dome co-culture, showing fibroblast markers (FAP, yellow) and the pericyte marker (PDGFRβ, green) in the presence of RFP + LCOs and DAPI staining. White arrows indicate FAP expression in BVOs. Quantification of fluorescence intensity shows the co-localization of FAP and PDGFRβ. (**E**) Schematic representation of the EMT process occurring in the LCO and BVO co-culture system. Illustrations were created with BioRender. Statistical significance was evaluated by two-tailed unpaired t-test (**A**) and one-way ANOVA (**B**, **C**, **D**) followed by a post hoc test with $^{*}p < 0.05$, $^{**}p < 0.01$, $^{***}p < 0.001$, and $^{****}p < 0.0001$.

upregulated in some LCOs migrating within VLCOs, despite being absent in LCO monocultures (Fig. 3G). Thus, in the VLCO model, LCOs undergo EMT while migrating along the BVO vasculature.

Beyond TGF-β signaling, hypoxia also induces EMT through hypoxia-inducible factors (HIFs)[26–28]. Therefore, we examined HIF-1α expression in VLCOs, finding it present in RFP-labeled LCOs within VLCOs but absent in LCO monocultures (Fig. 3H). HIF-2α was undetected under both conditions. The selective, significant increase of HIF-1α in VLCO, without induction of HIF-2α (a marker of chronic hypoxic adaptation) indicates a predominance of the acute hypoxia response. These results suggest that VLCOs induce EMT in LCOs via TGF-β signaling and HIF-1α expression, likely due to the hypoxic environment in VLCOs.

Stromal remodeling and fibrosis in VLCOs

We also analyzed stromal changes in VLCOs and observed extensive pericyte recruitment around LCO clusters (Fig. 4A), with their presence at the tumor–stroma interface suggesting active neovascularization and ECM remodeling. This was accompanied by increased CAF differentiation, marked by elevated expression of the

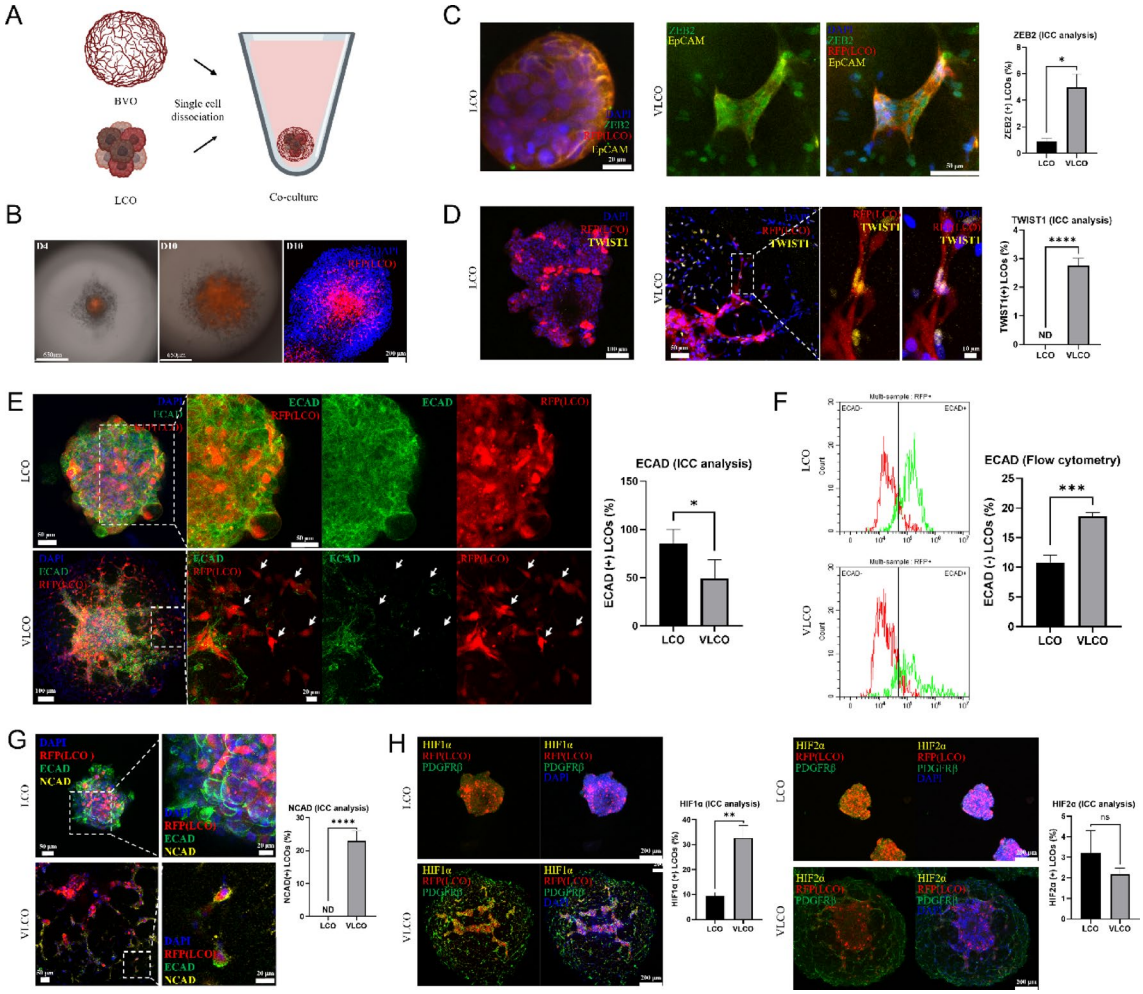

Fig. 3. Establishment of VLCOs and analysis of EMT-related characteristics. (**A**) Schematic representation of the establishment of vascularized lung cancer organoids. Illustrations were created with BioRender. (**B**) Bright-field and fluorescence images of RFP + LCOs in VLCOs at day 4 and day 10 after formation. (**C**) Immunofluorescence analysis of ZEB2 (green), EpCAM (yellow), RFP + LCOs, and DAPI staining in LCOs and VLCOs at day 10. (D) Immunofluorescence analysis of TWIST1 (yellow), RFP + LCOs, and DAPI staining in LCOs and VLCOs at day 10. Enlarged images showing the expression of TWSIT1 in LCOs. Dashed white boxes indicate regions shown at higher magnification in the adjacent panels. (**E**) Immunofluorescence imaging of ECAD (green) expression patterns between LCOs and VLCOs. White arrows indicated the negative expression of ECAD in LCOs. Dashed white boxes indicate regions shown at higher magnification in the adjacent panels. (**F**) Flow cytometry were performed the percentage of ECAD negative LCOs in VLCOs compared to LCOs. (**G**) Immunofluorescence analysis of N-cadherin (NCAD, yellow), E-cadherin (ECAD, green), RFP + LCOs, and DAPI staining in LCOs and VLCOs at day 10. Dashed white boxes indicate regions shown at higher magnification in the adjacent panels. (**H**) Immunofluorescence analysis of HIF1α (yellow), HIF2α (yellow) RFP + LCOs, and DAPI staining in LCOs and VLCOs at day 10. Statistical significance was evaluated by two-tailed unpaired t-test with $^{***}p < 0.001$.

fibroblast markers FSP1 and FAP (Fig. 4B, C)[29–31], with such differentiation being absent in BVO monocultures. These changes may contribute to prometastatic niche formation, supporting tumor growth and metastasis[32]. Notably, FSP1-positive CAF-like cells clustered around LCOs, indicating enhanced CAF differentiation near tumor cells.

Next, we investigated tumor fibrosis in VLCOs, a hallmark of stromal remodeling, characterized by accumulation of ECM components, including fibronectin, collagen I, and collagen III[33]. Fibronectin was absent in LCO monocultures but detected around LCOs in VLCOs (Fig. 4D). Similarly, collagen I and III, undetected in monocultured LCOs, were present in BVOs, primarily at their periphery (Fig. 4E). Collagen deposition followed a similar pattern in VLCOs, forming peripheral collagen-rich barriers. Taken together, these findings demonstrate that VLCOs recapitulate key TME features, including pericyte recruitment, CAF differentiation, and fibrosis.

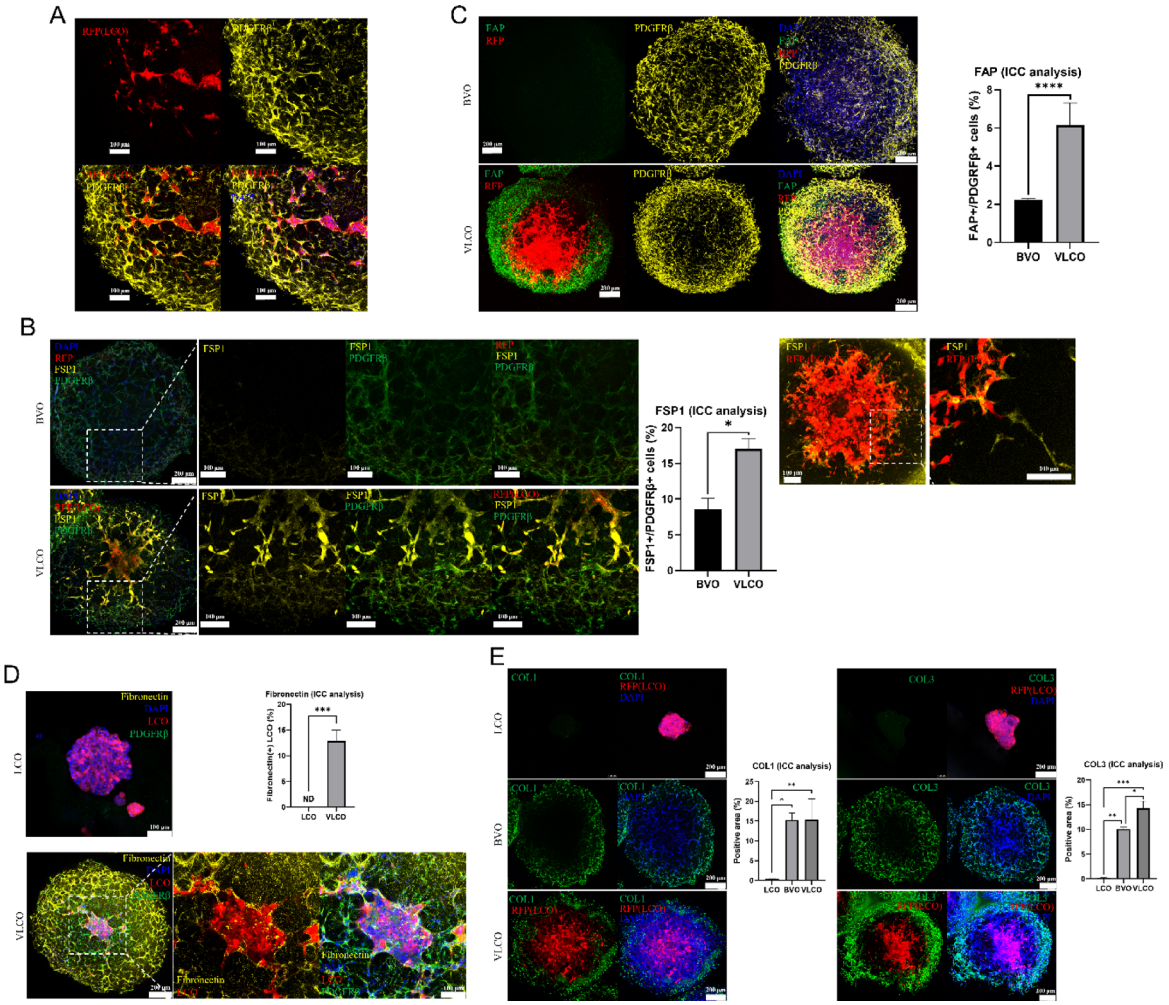

Fig. 4. Analysis of stromal remodeling and fibrosis in the VLCO model. (**A**) Immunofluorescence analysis of PDGFRβ (yellow), RFP + LCOs, and DAPI staining in VLCOs at day 10. (**B**) Immunofluorescence analysis of FSP1 (yellow), PDGFRβ (green), RFP + LCOs, and DAPI staining in BVOs and VLCOs at day 10. Graph shows % of PDGFRβ + cells co-expressing FSP1. Dashed white boxes indicate regions shown at higher magnification in the adjacent panels; the left panels show the magnified views. (**C**) Immunofluorescence analysis of FAP (green), RFP + LCOs, and DAPI staining in BVOs and VLCOs at day 10. Co-localization of PDGFRβ with FAP in BVOs by ICC. Graph shows % of PDGFRβ + cells co-expressing FAP. (**D**) Immunofluorescence analysis of Fibronectin (yellow), PDGFRβ (green), RFP + LCOs, and DAPI staining in LCOs and VLCOs at day 10. Dashed white boxes indicate regions shown at higher magnification in the adjacent panels. (**E**) Immunofluorescence analysis of Collagen1 and 3 (green), RFP + LCOs, and DAPI staining in LCOs, BVOs and VLCOs at day 10. Dashed white boxes indicate regions shown at higher magnification in the adjacent panels. Statistical significance was evaluated by one-way ANOVA(B) followed by a post hoc test with $^{**}p < 0.01$ and $^{****}p < 0.0001$.

Drug response assay established using VLCOs

We applied the VLCO model to a drug response assay for vasculature-induced EMT. As a proof-of-principle, we assessed the model's response to anti-EMT therapy employing galunisertib, a TGF-β1 receptor inhibitor. VLCOs were established using four RFP-labeled LCO lines: two EMT-prone LCOs (029T and 077 T) and two non-EMT LCOs (136T and 3057 T). LCOs exhibiting EMT began migrating along blood vessels by day 5, whereas non-EMT LCOs remained spherical clusters with minimal movement until at least day 7 (Figure S3). Therefore, we administered galunisertib on day 5, when EMT features became apparent. VLCOs were treated at three concentrations (1, 10, and 25 μM), with controls remaining untreated (0 μM).

To assess galunisertib's effect on EMT, we measured the RFP + LCO area on day 10. Using confocal imaging, we found that higher galunisertib concentrations reduced RFP-labeled cell dispersion in VLCOs derived from EMT-prone LCOs (Fig. 5A). Furthermore, quantitative image analysis confirmed a significant reduction in dispersed cell area in treated groups versus controls (Fig. 5B). However, VLCOs from non-EMT LCOs retained a clustered morphology, with no significant difference observed between groups. Galunisertib suppressed BVO growth at 25 μM but not at lower concentrations (Fig. 5C). However, an apoptosis assay indicated no significant

difference between the control and 25 μM–treated groups, suggesting that reduced size at high doses was not due to cell death (Figure S4). These results confirm VLCOs as a viable in vitro platform for screening vasculature-induced EMT in cancer cells. To verify galunisertib's inhibition of TGF-β signaling, we measured TGF-β1levels in the culture medium using ELISA (Fig. 5D). Compared with controls, treated VLCOs showed significantly lower TGF-β1 concentrations, confirming pathway inhibition. Assessing the expression of *TGF-β1* and genes involved in EMT and stromal remodeling, including *MMP2*, *FAP*, *Fibronectin*, *COL3A1*, and *FSP1* (Fig. 5E), qPCR analysis at 25 μM showed that *TGF-β1*, *MMP2*, *FAP*, and *Fibronectin* levels were reduced in all four VLCO models relative to control levels. In contrast, *COL3A1* and *FSP1* expression levels varied by LCO line, indicating variable responses to TGF-β inhibition.

We further tested the VLCO model's utility as a drug screening platform using the anti-VEGF monoclonal antibody bevacizumab, assessing its antiangiogenic effects. At high doses, bevacizumab significantly inhibited BVO proliferation, as evidenced by reduced VLCO size (Figure S5A, B). Notably, decreases in vascularization and LCO migration were correlated, highlighting a link between endothelial cell growth and tumor invasiveness. Additionally, qPCR analysis confirmed downregulation of angiogenesis- and EMT-related genes, reinforcing the BVOs' role in EMT induction in LCOs (Figure S5C). Collectively, these findings underscore the importance of vascular components in driving EMT and further support the VLCO model's utility as a vasculature-targeted anticancer therapy platform.

Long-term culture induces EMT in VLCOs

After characterizing VLCO behavior during early culture, we explored the effects of prolonged culture on their phenotype. Over time, VLCOs grew substantially, with bright-field images on day 32 showing markedly larger organoids compared with those on day 10 (Fig. 6A). To assess temporal changes in epithelial characteristics, we measured E-cadherin expression at various time points. On day 10, RFP-positive LCOs within VLCOs showed some E-cadherin expression, but by day 32, it was markedly reduced, indicating a loss of epithelial identity (Fig. 6B). Flow cytometry confirmed a gradual increase in the proportion of E-cadherin–negative, RFP-positive cells from day 10 to day 32 (Fig. 6C). Immunocytochemical staining also revealed higher N-cadherin levels in day-32 VLCOs (Fig. 6D), confirming the mesenchymal shift over extended culture. These findings indicate that long-term culture of VLCOs further promotes EMT.

Discussion

The VLCO model developed in this study mimics key aspects of the in vivo TME through LCO–BVO coculture. Examining these organoids' interactions, we found that vascularization promotes EMT in cancer cells and facilitates stromal remodeling, both critical for tumor progression. Additionally, we validated the VLCO model as a drug evaluation platform by assessing its response to the TGF-β inhibitor galunisertib, which effectively modulated EMT-related changes.

The established 3D tumor–vasculature coculture model recapitulated interactions in the TME, including pericyte recruitment, PFT, and fibroblast activation {Yang, 2016 #46}{Hosaka, 2016 #45}. These processes enhanced EMT in LCOs, highlighting tumor–stroma crosstalk's impact on cancer malignancy. Although our study focused on PFT as a key vascular remodeling mechanism, EndMT may also shape the VLCO microenvironment. EndMT has been implicated in tumor fibrosis and metastatic progression, suggesting that its relationships with EMT, pericyte recruitment, and fibroblast activation warrant further investigation, potentially offering novel antifibrotic and antimetastatic therapeutic opportunities {Zeisberg, 2007 #47}{Clere, 2020 #48} {Yin, 2023 #49}.

Beyond these therapies, VLCOs could aid in drug screening for EMT-driven cancers, often linked to increased drug resistance[34]. This model could facilitate testing of novel EMT-targeting therapies and evaluate treatment efficacy in EMT-driven lung cancers. Furthermore, VLCOs could enable combination therapy studies, such as vasculature-targeted therapies with lung cancer–specific treatments (e.g., EGFR-TKIs) or EMT inhibitors with standard lung cancer therapies. By providing a 3D, physiologically relevant model, VLCO-based drug screening could accelerate preclinical drug development and support personalized medicine in lung cancer treatment.

Our study also revealed phenotypic diversity among patient-derived LCOs, suggesting that VLCOs could help predict tumor progression. Of the tested LCOs, two pleural effusion–derived samples (029T and 077T) exhibited EMT, whereas another such sample (136T) did not. These findings suggest that tumors from the same anatomical site may exhibit distinct metastatic potentials. Through analysis of EMT features in VLCOs, the platform holds value for evaluating LCO aggressiveness and predicting treatment outcomes in lung cancer. Expanding VLCO studies with a larger sample of patient-derived LCOs and BVOs may elucidate relationships among EMT patterns, molecular characteristics, and drug responsiveness. Additionally, multi-omics analyses could provide deeper insights into the molecular mechanisms underlying EMT induction in this system.

Limitations of the VLCO model

Despite its advantages, the VLCO model has limitations, especially regarding replicating the full complexity of the in vivo TME. Although our coculture system includes cancer organoids, endothelial cells, pericytes, and mesenchymal stem cells, it lacks immune cells, neural components, and diverse fibroblast subtypes, which influence tumor progression in ways that our model cannot capture. Additionally, although Matrigel-based 3D cultures support vascular network formation, they do not fully replicate in vivo biophysical conditions, including shear stress, nutrient gradients, and matrix stiffness, owing to the absence of actual blood flow. Incorporating techniques such as single-cell RNA sequencing to analyze EMT dynamics and cell–cell interactions could improve the model's relevance to in vivo tumor biology.

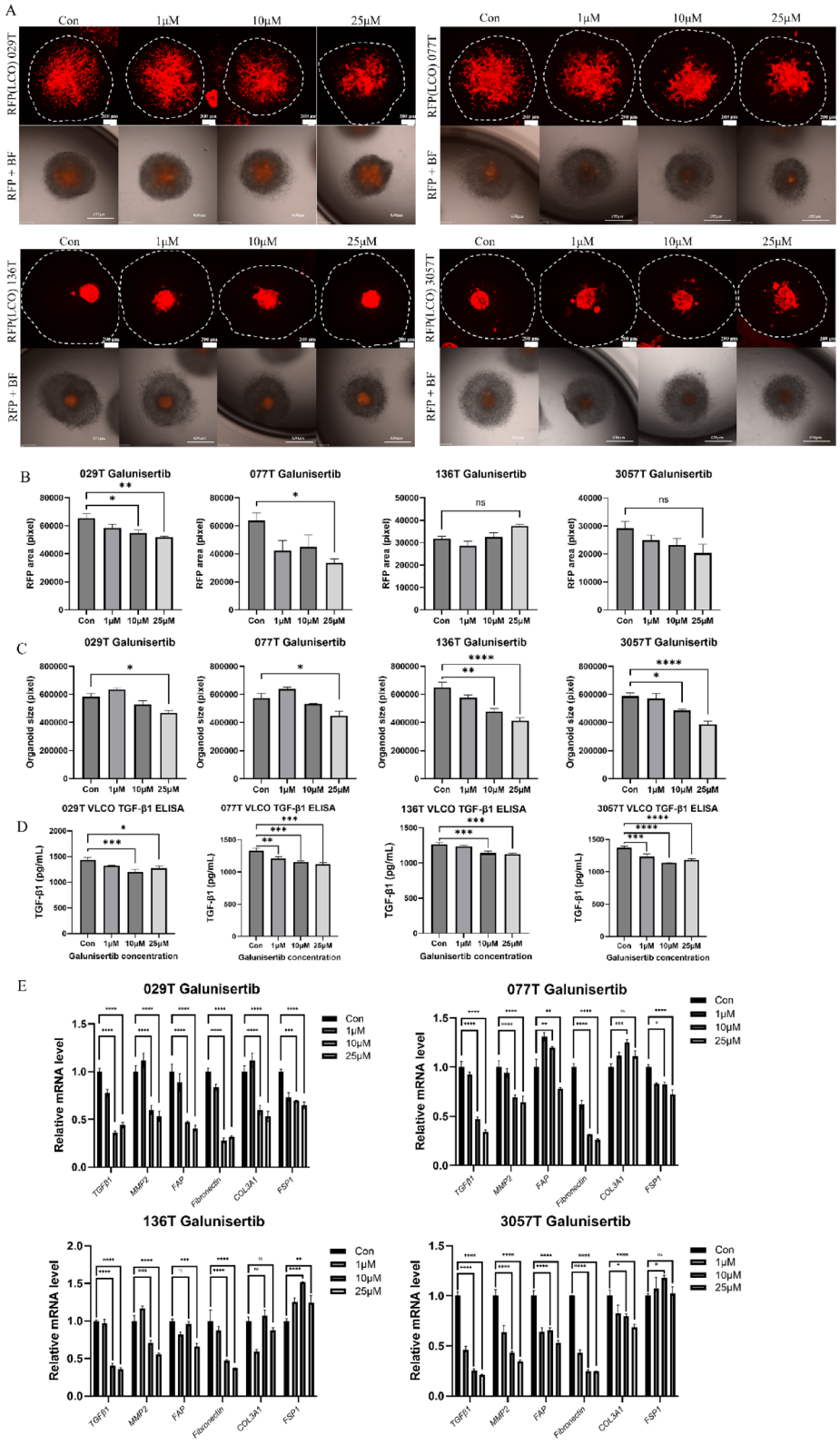

Conclusions

In this study, we established a VLCO model by coculturing LCOs and BVOs in a 3D in vitro system, successfully recapitulating tumor–vasculature interactions. This platform enabled assessment of EMT induction, PFT, and stromal remodeling, as well as therapeutic evaluations of anti-EMT and antiangiogenic treatments. Overall, our findings enhance understanding of lung cancer progression and demonstrate that VLCOs are a valuable model for drug discovery and personalized medicine.

◀**Fig. 5**. Drug evaluation test of Galunisertib (TGF-β1 receptor inhibitor) using VLCO model. (**A**) Confocal, bright-field, and fluorescence images of VLCOs derived from four LCO types (029T, 077 T, 136 T, 3057 T) at day 10 following Galunisertib treatment at concentrations of control (0 μM), 1 μM, 10 μM, and 25 μM. (**B**) Quantification of the RFP-positive area within the VLCO region at day 10, based on the experimental conditions described in Fig. 5A. (**C**) Image-based organoid size measurements at day 10 under the same conditions outlined in Fig. 5A. Quantification of the organoid size of VLCO using image-based analysis. (**D**) TGF-β1 levels measured by ELISA assay at day 10, following the same conditions described in Fig. 5A. (**E**) qPCR analysis of *TGFβ1*, *MMP2*, *FAP*, *Fibronectin*, *COL3A1*, and *FSP1* expression in VLCOs at day 10, conducted under the same experimental conditions detailed in Fig. 5A. All gene expression values were normalized to *GAPDH*. Statistical significance was evaluated by one-way ANOVA (**B**, **C**, **D**) and two-way ANOVA(E) followed by a post hoc test, with $*p<0.05$, $**p<0.01$, $***p<0.001$, and $****p<0.0001$.

Material and methods

Culture of HiPSCs

The following cell lines were obtained from the CIRM hPSC Repository funded by the California Institute of Regenerative Medicine (CIRM): [CW50028]. Human induced pluripotent stem cells (hiPSCs) were maintained on 6well culture plates (Corning, 3516, Durham, NC, USA) pre-coated with Vitronectin XFTM (StemCell Technologies, 07180, Vancouver, Canada) according to the manufacturer's instructions. The cells were cultured in StemFit™ Basic04 CT medium (Ajinomoto, AJBASIC04CT, Tokyo, Japan), which was replaced daily. When the hiPSCs reached approximately 70% confluency, the cells were passaged. For passaging, the medium was aspirated, and cells were washed once with phosphate-buffered saline (PBS) (Gibco, Thermo Fisher Scientific, 14190-250, Waltham, MA, USA). Subsequently, 5mM EDTA (Invitrogen, AM9260G, Carlsbad, CA, USA) was added and incubated for 5 min at 37 °C to dissociate the cells. The EDTA solution was then neutralized by adding an equal volume of StemFit™ Basic04 CT medium (Ajinomoto). The cell suspension was gently pipetted to create a single-cell suspension and transferred to a new Vitronectin XFTM (StemCell Technologies)-coated culture plate containing fresh StemFit™ Basic04 CT medium (Ajinomoto). All cultures were maintained at 37 °C in a 5% CO_2 humidified incubator (Thermo Fisher Scientific, 371), and medium was changed every day. Cells used for all experiments are between passage 15 ~ 25.

Differentiation of BVO

When the hiPSCs were reached at 70% confluency, cells were dissociated into single cells with Accutase (Gibco, 07922) for 5 min at 37 °C. To inactivate the enzymatic reaction, an equal volume of StemFit™ Basic04 CT medium (Ajinomoto) was added in dissociated cells. Then these cells were resuspended in the aggregation medium [KnockOut™ DMEM/F-12 medium (Gibco, 12660012), 20% KnockOut™ Serum Replacement (Gibco, 10828028), 1X Glutamax (Gibco, 35050061), 1X NEAA (Gibco, 11140035), 2-Mercaptoethanol (Gibco, 21985023), 1% Penicillin-Streptomycin (Gibco, 15140122) with 50μM Y27632 (Tocris Bioscience, 1254, Bristol, UK)] and seeded into the PrimeSurface® V-bottom 96well plate (Sumitomo Bakelite Co., Ltd., MS-9096VZ, Tokyo, Japan) with 3,000 cells per each well. To form a single aggregate in each well, centrifugated 1,000 rpm for 1 min. On day 1, the aggregation medium was replaced by the mesodermal induction medium, which is consist of N2B27 basal medium [DMEM/F-12, HEPES (Gibco, 11330032), Neurobasal™ medium (Gibco, 21103049) (1:1), 1X N-2 Supplement (Gibco, 17502048), 1X B-27 Supplement, minus vitamin A (Gibco, 12587010), 1X Glutamax (Gibco), 2-Mercaptoethanol (Gibco), 1% Penicillin-Streptomycin (Gibco)] with 12μM CHIR99021 (Tocris Bioscience, 4423), 30ng/mL BMP4 (Miltenyi Biotec, 130-111-165, Bergisch Gladbach, Germany). On day 4, the mesodermal induction medium was replaced by the vascular induction medium, which is consist of N2B27 basal medium with 100ng/mL VEGF-A (PeproTech, 100-18b, Rocky Hill, NJ, USA), 2μM Forskolin (Sigma-Aldrich, F3917, St. Louis, MO, USA) and cultured for 2days. On day 6, vascular-induced aggregates were embedding into Matrigel (Corning, 354230)/collagen Ⅰ (Advanced BioMatrix Inc., 5005, Carlsbad, CA, USA) gels in 12well culture plate (Corning, 3512) to form vascular networks. medium was replaced by BVO maturation medium containing StemPRO-34 complete medium (Gibco, 10639011), 1X Glutamax (Gibco) with 100ng/mL VEGF-A (PeproTech) and 100ng/mL bFGF (PeproTech). medium was changed every second to third day. On day 11, vascular networks were extracted from the Matrigel/collagen Ⅰ (1:1) gels using spatula (AS ONE, 6–524-05, Osaka, Japan) and 25 g needles (Jung Rim Medical Industrial Co., Ltd., JRN-25G, Seoul, Republic of Korea). Single vascular networks were seeding into each well of V-bottom 96well plate (Sumitomo Bakelite Co., Ltd.). medium was replaced by BVO maturation medium and changed every second to third day. After cultured for 4 ~ 5 days, these vascular networks self-assembled into BVOs and could be cultured for up to 1 month.

Patients samples acquisition and ethical approval

This study was approved by Yonsei University Hospital Institutional Review Board (Seoul, Korea; IRB no.: 4–2016-0788) and Samsung Medical Center Institutional Review Board (Seoul, Korea, IRB no.: 2022-12-083-001). All participants provided written informed consent according to the Declaration of Helsinki. Pleural effusion samples were collected from patients with advanced lung adenocarcinoma at Yonsei Cancer Center, and surgically resected tumor sample was collected from a patient with squamous cell carcinoma at Samsung Medical Center.

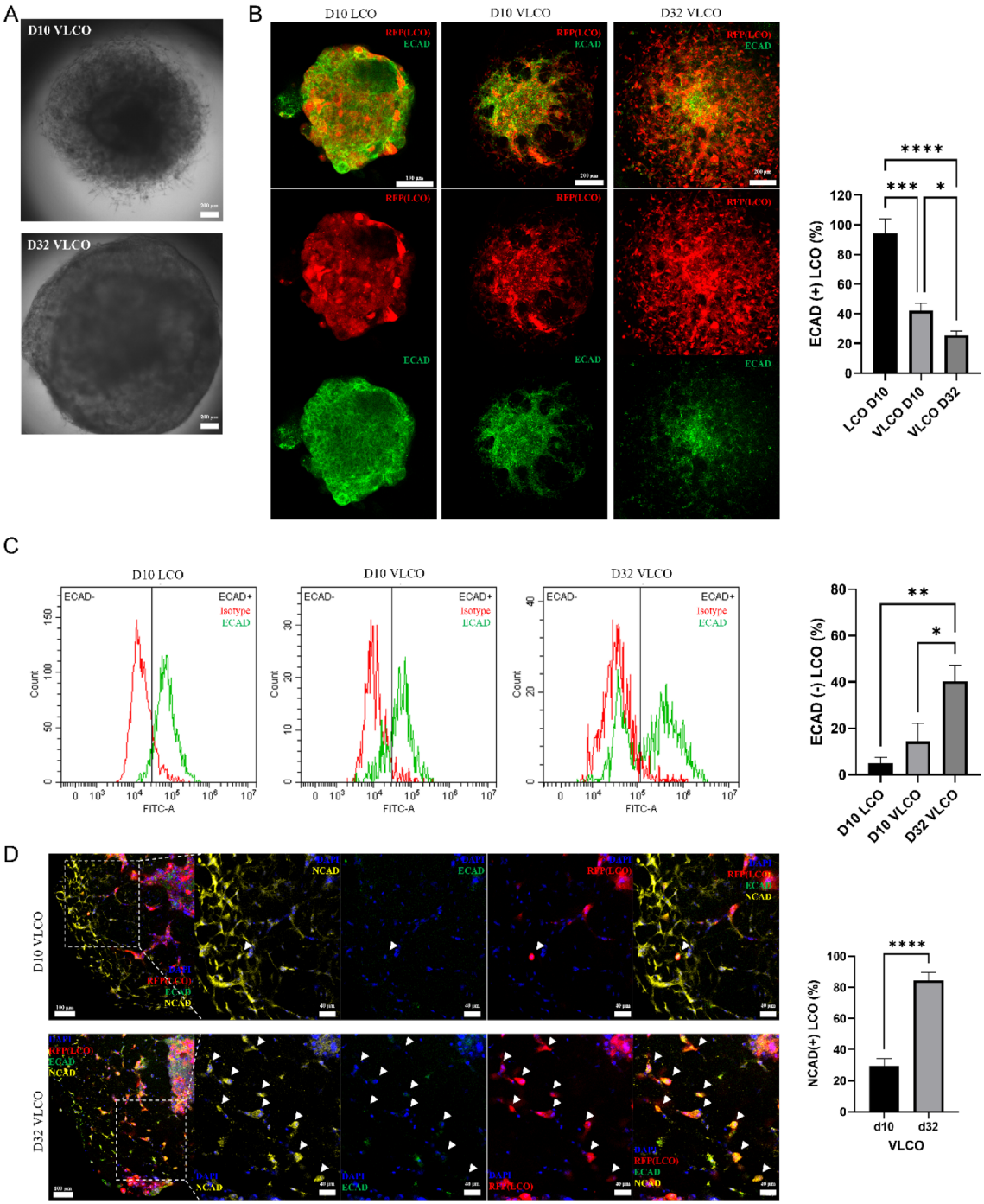

Fig. 6. Analysis of EMT characteristics of long-term cultured VLCOs. (**A**) Bright-field images of D10 and D32 VLCOs. (**B**) Immunofluorescence imaging of D10 LCO (left), D10 VLCO (center), D32 VLCO (right) for the expression of E-cadherin (green). Dashed white boxes indicate regions shown at higher magnification in the adjacent panels. (**C**) Flow cytometry analysis of ECAD with quantification of the ECAD^{-}/RFP LCOs in VLCOs (D10, D32). Representative flow cytometry plots of ECAD expression (green line) compared with isotype control (red line). (**D**) Immunofluorescence imaging of VLCOs (D10, D32) for the expression of ECAD (green) and NCAD (yellow). Arrow heads were indicated the NCAD^{+}/RFP LCOs. Quantification of fluorescence intensity shows that NCAD positive LCOs. Dashed white boxes indicate regions shown at higher magnification in the adjacent panels. Statistical significance was evaluated by two-way ANOVA followed by a post hoc test (**B**, **C**) two-tailed unpaired t-test (**D**) with $^{*}p < 0.05$, $^{**}p < 0.01$, $^{***}p < 0.001$, and $^{****}p < 0.0001$.

Isolation and processing of malignant effusions and surgical tumor tissues

Pleural effusion samples were centrifuged at 450 ×g for 3 min at 4 °C to remove cell debris. Red blood cells were lysed using MilliQ H_2O (Merk Millipore Darmstadt, Germany), followed by the addition of Advanced DMEM/F12 (Gibco) to neutralize the lysis. The suspension was then filtered through a 100 μm filter and centrifuged again at 450 ×g for 3 min at 4 °C.

Surgical tumor tissue was transported in cold DMEM/F-12 medium supplemented with antibiotics. Upon arrival, the tissue was washed with Advanced DMEM/F12 to remove debris and contaminants. The washed tissue was then minced into small fragments (1–2 mm^3) using a sterile blade and subjected to enzymatic digestion in Complete Medium containing 2 mg/mL collagenase (Sigma-Aldrich, C9407) at 37 °C for 60 min with continuous agitation. The cell suspension was then supplemented with Advanced DMEM/F12, filtered through a 100 μm strainer, and centrifuged at 450 ×g for 3 min at 4 °C.

Organoid maintenance and expansion

The isolated cells were mixed with Matrigel at a 1:1 ratio and seeded in 24-well plates as dome-shaped droplets. After gelation at 37 °C for 15 min, the droplets were overlaid with complete organoid culture medium supplemented with growth factors, including recombinant R-Spondin1{Gradiant Bioconvergence Inc. (GBCC) production}, B-27 (Gibco), human FGF10 (GBCC), human FGF7 (GBCC), human Noggin (GBCC), N-acetylcysteine (Sigma), SB202190 (Sigma), A83-01 (Tocris), human Gastrin I (Sigma), human Heregulinβ−1 (Peprotech), Nutlin3a (Cayman Chemical, Ann Arbor, MI, USA), Wnt3a conditioned medium (GBCC) and Primocin (InvivoGen, San Diego, CA, USA). The culture medium was replaced every 2–3 days.

Organoids were monitored daily for growth and morphology. Once established, they were passaged every 7–14 days using mechanical dissociation and gentle enzymatic digestion with TrypLE Express (Gibco). The fragmented organoids were re-embedded in fresh Matrigel and maintained under the same culture conditions.

Single cell dissociation

Organoids were washed twice with PBS (Gibco) to remove any residual medium. LCOs were dissociated by 0.05% trypsin-EDTA(Gibco) and BVOs were dissociated by the enzyme mixture which is consist of 3 U ml − 1 dispase (Gibco, 17105041), 2 U ml − 1 Liberase™ TH Research Grade (Roche, 5401135001, Basel, Switzerland) and 100 U DNase (Stemcell Tech, 07900) in PBS (Gibco) for 20 min at 37 °C water bath. To halt the enzymatic reaction, an equal volume of 10% FBS (Gibco) medium in Advanced DMEM/F-12 (Gibco) was added in dissociated cells and gently pipetting to obtain a single cell suspension and strained using a Falcon® 70 μm Cell Strainer (Corning, 35230). The dissociated cells were used at varying cell numbers according to the requirements of each experiment.

Co-culture of LCOs and BVOs in matrigel dome

LCOs and BVOs were co-cultured in a Matrigel dome to establish a three-dimensional interaction model. LCOs were mechanically dissociated into small clumps, and approximately 100 LCO clumps were used per culture. BVOs were dissociated into single cells, and 2000 BVO cells were suspended in 50 μL of Matrigel. The mixture was seeded onto a culture dish and incubated at 37 °C for polymerization before adding culture medium. The co-culture was maintained under standard organoid culture conditions for further analysis.

Intravasation assay

First of all, LCOs were dissociated into single cells by previous described in sing cell dissociation method. 3,000 cells of LCO were cocultured with BVO on Ultra-Low Attachment 96 Well Plate (Corning, 7007). Coculture medium, consist of LCO, BVO maturation medium (1:1) were used and cocultured for 7 ~ 16 days depends on experiments.

Immunocytochemistry

Organoids was fixed in 4% paraformaldehyde (Biosesang, PC2031-050-00, Gyeonggi-do, Republic of Korea) for 15 min (Matrigel dome culture) or 1 h (V-bottom culture) at room temperature. The fixed samples were blocked and permeabilized using with 3% FBS (Gibco, 16000044), 1% BSA (Sigma-Aldrich, A2153), 0.5% Triton X-100(Sigma-Aldrich, 93443), 0.5% tween-20 (Sigma-Aldrich, P2287) in PBS (Gibco) for 5 h at room temperature on a shaker. Primary antibodies were diluted 1:100 ~ 200 in blocking buffer and incubated for 3days at 4 °C. The following primary antibodies were used in this study: CD31 (R&D systems, AF806), PDGFRβ (Cell signaling, 3169 S, Danvers, MA, USA; R&D systems, AF385, Minneapolis, MN, USA), Fibronectin (Cell signaling, 26836 S), Collagen type Ⅰ (Cell signaling, 72026 S), Collagen type Ⅲ (Cell signaling, 66887 S), Collagen type IV (Sigma-Aldrich, AB769), FSP1 (R&D systems, MAB4137; Invitrogen, MA5-31332), FAP (Invitrogen, PA5-51057), ECAD (BD Bioscience, BD562869; Cell signaling, 14472 S), NCAD (Cell signaling, 13116 S; R&D systems, AF6426), EpCAM (Cell signaling, 2929 S), TWIST1 (Cell signaling, 90445 S), ZEB2 (Invitrogen, PA5-20980), SOX2 (Sigma-Aldrich, AB5603), NANOG (MBL Life science, PM058, Tokyo, Japan). After organoids were washed for three times in PBST buffer. And secondary antibodies were diluted 1:500 and incubated for 1 day at 4 °C. The following secondary antibodies were used in this study: Donkey anti-mouse Alexa Flour™ 488 (Jackson ImmunoResearch, 715-545-151), Donkey anti-mouse Alexa Flour™ 555 (Invitrogen, A-31570), Donkey anti-mouse Alexa Flour™ 647 (Jackson ImmunoResearch, 715-605-151), Donkey anti-rabbit Alexa Flour™ 488, Jackson ImmunoResearch, 711-545-152), Donkey anti-rabbit Alexa Flour™ 555 (Invitrogen, A-31572), Donkey anti-rabbit Alexa Flour™ 647 (Jackson ImmunoResearch, 711-605-152), Donkey anti-goat Alexa Flour™ 488 (Jackson ImmunoResearch, 705-545-147), Donkey anti-goat Alexa Flour™ 647 (Jackson ImmunoResearch, 705-605-147), Donkey anti-sheep Alexa Flour™ 488 (Invitrogen, A-11015), Donkey anti-sheep Alexa Flour™ 647 (Invitrogen, A-21448). After organoids were washed for three times in PBS(Gibco).

Finally, organoids were diluted 1:1000 in DAPI solution (Thermo Fisher Scientific, 62248) for nuclear staining. Organoids were incubated in RapiClear® 1.47 (SunJinLab, RC147002, Hsinchu City, Taiwan) for clearing. And mounted in iSpacer® 1.0 mm (SunJinLab, IS018), incubated for overnight at room temperature. After 1 day, images were analyzed by confocal microscope (Carl Zeiss, Oberkochen, Germany) and processed by the ImageJ program. We have described the list of antibodies in Table S1.

Quantitative real-time polymerase chain reaction

Total RNA from pooled Matrigel dome culture organoids or vascularized cancer organoids was isolated using an RNeasy Plus Kits for RNA isolation (Qiagen, Hilden, Germany) following the manufacturer's instructions. cDNA was synthesized using a HighCapacity RNA-to-cDNA Kit (Applied Biosystems, Foster City, CA, USA). The cDNA samples were amplified using Power SYBR Green Master Mix (Applied Biosystems) containing 1 pmol of each primer set listed in Table S2 in a 10 μL reaction volume. Amplification and detection were conducted using the QuantStudio 3 Real-Time PCR Instrument (Applied Biosystems) under the following conditions: one cycle of 50 °C for 2 min and 95 °C for 10 min, followed by 40 cycles of denaturation at 95 °C for 15 s and annealing/extension for 1 min (annealing/extension temperatures were dependent on each primer set). The dissociation curves were analyzed, and the amplified products were loaded onto gels to confirm the specificity of the PCR products. The relative expression level was calculated by normalizing the threshold cycle (Ct) values of each gene to that of the reference gene Glyceraldehyde 3-phosphate dehydrogenase (GAPDH) via the delta-delta Ct method.

Enzyme-linked immunosorbent assay (ELISA)

To quantify the levels of secreted TGF-β1, TGF-β2, and PDGF-BB, culture supernatants were collected from LCO, BVO, and VLCO groups at the indicated time points. The concentrations of these factors were measured using commercial ELISA kits from R&D Systems (R&D Systems, Minneapolis, MN, USA) following the manufacturer's protocol. Briefly, activated samples and standards were added to pre-coated 96-well plates according to the manufacturer's protocol and incubated at room temperature for 2 h. After washing steps, wells were incubated with the detection antibody for 2 h at room temperature, followed by the addition of the substrate solution and incubation for 30 min in the dark. The reaction was stopped with a stop solution, and the optical density was measured at 450 nm using a microplate reader (model, manufacturer). For each condition, $n = 3$ independent biological replicates were analyzed. All samples were analyzed in technical duplicates, and data were normalized to total protein concentration.

Flow cytometry

To make the organoids into single cells, organoids were dissociated using as previously described. Single cells were washed with Cell Staining Buffer (Biolegend, 420201, San Diego, CA, USA) and stained with fluorescence conjugated antibody for 1 h at 4 °C. The following antibodies were used in this study: Alexa Fluor® 488 Mouse IgG1 κ Isotype Control (BD Biosciences, 557782), Alexa Fluor® 488 Mouse anti-E-Cadherin (BD Biosciences, 560061). Cells were washed with cell staining buffer and stained with DAPI solution (Gibco) for 10 min at 4 °C. Finally, cells were analyzed by CytoFLEX Flow cytometer (Beckman Coulter, B53010, Brea, CA, USA).

Image based assay

Fluorescence intensity and organoid size were quantified using ImageJ software (NIH, Bethesda, MD, USA). For each condition, $n = 5$ independent biological replicates were analyzed; within each replicate, 5 non-overlapping fields/organoids were quantified. For fluorescence analysis, regions of interest were selected, and mean gray values were measured, with background fluorescence subtracted to obtain corrected total fluorescence intensity. Organoid size was measured by outlining the organoid boundaries and calculating the corresponding area.

Generation of VLCOs

To make the LCOs and BVOs into single cells, organoids were dissociated using as previously described. 2,000 cells derived from LCOs and 2,000 cells derived from BVOs are combined in the 15mL conical tube. And centrifuge at 450 g for 5 min, discard supernatants and add the coculture medium which is consist of LCO medium and BVO maturation medium with 50ng/mL VEGF-A (PeproTech) and 5% Matrigel (Corning). Mixed cells were seeding into the PrimeSurface® V-bottom 96well plate (Sumitomo Bakelite Co., Ltd.) and centrifuge at 450 g for 5 min to facilitate VLCO formation. The VLCOs were then cultured for 10 days or 32 days in a 37 °C hypoxic incubator with 5% CO_2 and high humidity.

Drug treatment assay and sample collection

To evaluate the effects of Galunisertib on VLCOs, drug treatment was initiated on day 5 of VLCO culture. Galunisertib (MedChemExpress, Monmouth Junction, NJ, USA) was dissolved in DMSO and added to the culture medium at final concentrations of 1 μM, 10 μM, and 25 μM, with a control group receiving an equivalent volume of DMSO (0 μM). After five days of treatment, all samples were collected on day 10 for further analysis. On day 10, supernatants were collected for ELISA to measure TGF-β1 levels. RNA was isolated from VLCOs for qRT-PCR analysis to assess gene expression changes. Additionally, VLCOs were fixed for immunocytochemistry (ICC) to examine protein expression.

For bevacizumab treatment, VLCOs were cultured in 2% Matrigel to enhance the antibody's efficacy. On day 3 of culture, these VLCOs were then treated with bevacizumab (MedChemExpress, Monmouth Junction, NJ, USA) at final concentrations of 2 mg/mL and 3 mg/mL, while a control group received no treatment. Image-based analysis was performed by capturing images daily from day 4 to day 7. On day 7, RNA was isolated from VLCOs, and qRT-PCR analysis was conducted to assess gene expression changes.

Apoptosis assay (NucView 488 Staining)

Apoptosis in VLCOs was assessed using the NucView 488 Caspase-3 Assay Kit for Live Cells (Biotium, Fremont, CA, USA). VLCOswere incubated with 2 μM NucView 488 substrate at 37 °C for 1 h according to the manufacturer's instructions. After incubation,samples were imaged using a confocal microscope. Fluorescence intensity was quantified using ImageJ by measuring the mean grayvalue of regions of interest and subtracting background fluorescence to obtain corrected total cell fluorescence.

Statistical analysis

Statistical analysis of data was performed using GraphPad Prism Software (version 10). Significant differences in gene expression among the experimental groups were determined by one-way analysis of variance followed by Tukey's multiple-comparison test. Differences were considered significant at * $p < 0.05$, ** $p < 0.01$ *** $p < 0.001$ and **** $p < 0.0001$ in the figures. Data are presented as the mean ± standard error of the mean (SEM).

Data availability

The datasets used and/or analysed during the current study are available from the corresponding author on reasonable request. Supplementary Information accompanies this paper and includes additional figures, raw data, and detailed experimental procedures supporting the findings of this study.

Received: 4 August 2025; Accepted: 14 November 2025
Published online: 24 November 2025

References

1. Gupta, G. P. & Massagué, J. Cancer metastasis: Building a framework. *Cell* **127**, 679–695 (2006).
2. Fares, J., Fares, M. Y., Khachfe, H. H., Salhab, H. A. & Fares, Y. Molecular principles of metastasis: A hallmark of cancer revisited. *Signal. Transduct. Target. Therapy.* **5**, 28 (2020).
3. Hanahan, D. & Weinberg, R. A. Hallmarks of cancer: The next generation. *Cell* **144**, 646–674 (2011).
4. Folkman, J. Role of angiogenesis in tumor growth and metastasis. In *Seminars in Oncology* (Elsevier, 2002).
5. Hosaka, K. et al. Pericyte–fibroblast transition promotes tumor growth and metastasis. *Proceedings of the National Academy of Sciences* 113, E5618-E5627 (2016).
6. Zeisberg, E. M., Potenta, S., Xie, L., Zeisberg, M. & Kalluri, R. Discovery of endothelial to mesenchymal transition as a source for carcinoma-associated fibroblasts. *Cancer Res.* **67**, 10123–10128 (2007).
7. Yanagisawa, K. et al. A four-dimensional organoid system to visualize cancer cell vascular invasion. *Biology* **9**, 361 (2020).
8. Kwak, T. J. & Lee, E. In vitro modeling of solid tumor interactions with perfused blood vessels. *Sci. Rep.* **10**, 20142 (2020).
9. Wörsdörfer, P. et al. Generation of complex human organoid models including vascular networks by incorporation of mesodermal progenitor cells. *Sci. Rep.* **9**, 15663 (2019).
10. Wimmer, R. A. et al. Human blood vessel organoids as a model of diabetic vasculopathy. *Nature* **565**, 505–510 (2019).
11. Sun, X-Y. et al. Generation of vascularized brain organoids to study neurovascular interactions. *Elife* **11**, e76707 (2022).
12. Dao, L. et al. Modeling blood-brain barrier formation and cerebral cavernous malformations in human PSC-derived organoids. *Cell. Stem Cell.* **31**, 818–833 (2024).
13. Kong, D. et al. In vitro modeling of atherosclerosis using iPSC-derived blood vessel organoids. *Adv. Healthc. Mater.* **14**, 2400919 (2025).
14. Lancaster, M. A. & Knoblich, J. A. Organogenesis in a dish: Modeling development and disease using organoid technologies. *Science* **345**, 1247125 (2014).
15. Xu, H., Jiao, D., Liu, A. & Wu, K. Tumor organoids: Applications in cancer modeling and potentials in precision medicine. *J. Hematol. Oncol.* **15**, 58 (2022).
16. Kong, D. et al. CD19 CAR-expressing iPSC-derived NK cells effectively enhance migration and cytotoxicity into glioblastoma by targeting to the pericytes in tumor microenvironment. *Biomed. Pharmacother.* **174**, 116436 (2024).
17. Wimmer, R. A., Leopoldi, A., Aichinger, M., Kerjaschki, D. & Penninger, J. M. Generation of blood vessel organoids from human pluripotent stem cells. *Nat. Protoc.* **14**, 3082–3100 (2019).
18. Choudhury, J., Pandey, D., Chaturvedi, P. K. & Gupta, S. Epigenetic regulation of epithelial to mesenchymal transition: A trophoblast perspective. *Mol. Hum. Reprod.* **28**, gaac013 (2022).
19. Restivo, G. et al. The low affinity neurotrophin receptor CD271 regulates phenotype switching in melanoma. *Nat. Commun.* **8**, 1988 (2017).
20. Zhao, Z. et al. TGF-β promotes pericyte-myofibroblast transition in subretinal fibrosis through the Smad2/3 and Akt/mTOR pathways. *Exp. Mol. Med.* **54**, 673–684 (2022).
21. Chang, F-C., Chou, Y-H., Chen, Y-T. & Lin, S-L. Novel insights into pericyte–myofibroblast transition and therapeutic targets in renal fibrosis. *J. Formos. Med. Assoc.* **111**, 589–598 (2012).
22. Kim, B. N. et al. TGF-β induced EMT and stemness characteristics are associated with epigenetic regulation in lung cancer. *Sci. Rep.* **10**, 10597 (2020).
23. Yu, Y. et al. Cancer-associated fibroblasts induce epithelial–mesenchymal transition of breast cancer cells through paracrine TGF-β signalling. *Br. J. Cancer.* **110**, 724–732 (2014).
24. Shintani, Y. et al. IL-6 secreted from cancer-associated fibroblasts mediates chemoresistance in NSCLC by increasing epithelial-mesenchymal transition signaling. *J. Thorac. Oncol.* **11**, 1482–1492 (2016).
25. Zhang, H., Jiang, H., Zhu, L., Li, J. & Ma, S. Cancer-associated fibroblasts in non-small cell lung cancer: Recent advances and future perspectives. *Cancer Lett.* **514**, 38–47 (2021).
26. Chen, S. et al. Hypoxia induces TWIST-activated epithelial–mesenchymal transition and proliferation of pancreatic cancer cells in vitro and in nude mice. *Cancer Lett.* **383**, 73–84 (2016).
27. Cheng, J-C., Klausen, C. & Leung, P. C. Hypoxia-inducible factor 1 alpha mediates epidermal growth factor-induced down-regulation of E-cadherin expression and cell invasion in human ovarian cancer cells. *Cancer Lett.* **329**, 197–206 (2013).
28. Depner, C. et al. EphrinB2 repression through ZEB2 mediates tumour invasion and anti-angiogenic resistance. *Nat. Commun.* **7**, 12329 (2016).
29. Kraman, M. et al. Suppression of antitumor immunity by stromal cells expressing fibroblast activation protein–α. *Science* **330**, 827–830 (2010).
30. Kalluri, R. & Zeisberg, M. Fibroblasts in cancer. *Nat. Rev. Cancer* **6**, 392–401 (2006).
31. Chen, X. & Song, E. Turning foes to friends: Targeting cancer-associated fibroblasts. *Nat. Rev. Drug Discov.* **18**, 99–115 (2019).
32. Jiang, Z. et al. Pericytes in the tumor microenvironment. *Cancer Lett.* **556**, 216074 (2023).
33. Kai, F., Drain, A. P. & Weaver, V. M. The extracellular matrix modulates the metastatic journey. *Dev. Cell.* **49**, 332–346 (2019).

34. Du, B. & Shim, J. S. Targeting epithelial–mesenchymal transition (EMT) to overcome drug resistance in cancer. *Molecules* **21**, 965 (2016).

Author contributions

Mingyun, as the first author, led and performed the majority of the experiments. He was primarily responsible for Figs. 2, 3, 4 and 5, and 6, and contributed extensively to the generation and analysis of all supplementary data. Yeo-Joon, as the second author, developed the vascular organoids and was responsible for all data presented in Figure 1. Mina, Sewon, Min Hak, Sang-Won, and Byoung Chul Cho provided tumor tissue samples essential for the establishment of lung cancer organoids. They also performed genetic validation to confirm the cancerous identity of the established organoids and contributed to the analysis related to metastasis. Jinguen and Sato provided critical guidance on experimental design and helped organize and interpret the data. Yong-Soo, as the corresponding author, conceptualized the study, designed and supervised the experiments, and oversaw the overall project direction.

Declarations

Competing interests

The authors declare no competing interests.

Additional information

Supplementary Information The online version contains supplementary material available at https://doi.org/10.1038/s41598-025-29214-9.

Correspondence and requests for materials should be addressed to Y.S.L.

Reprints and permissions information is available at www.nature.com/reprints.

Publisher's note Springer Nature remains neutral with regard to jurisdictional claims in published maps and institutional affiliations.